PHYSICAL REVIEW D **91,** 054035 (2015)

Chiral symmetry breaking in continuum QCD

Mario Mitter,[1] Jan M. Pawlowski,[1,2] and Nils Strodthoff[1]

[1]*Institut für Theoretische Physik, Universität Heidelberg, Philosophenweg 16, 69120 Heidelberg, Germany*

[2]*ExtreMe Matter Institute EMMI, GSI, Planckstrasse 1, D-64291 Darmstadt, Germany*

(Received 18 December 2014; published 25 March 2015)

We present a quantitative analysis of chiral symmetry breaking in two-flavor continuum QCD in the quenched limit. The theory is set up at perturbative momenta, where asymptotic freedom leads to precise results. The evolution of QCD towards the hadronic phase is achieved by means of dynamical hadronization in the nonperturbative functional renormalization group approach. We use a vertex expansion scheme based on gauge-invariant operators and discuss its convergence properties and the remaining systematic errors. In particular, we present results for the quark propagator, the full tensor structure and momentum dependence of the quark-gluon vertex, and the four-Fermi scatterings.

DOI: 10.1103/PhysRevD.91.054035 PACS numbers: 12.38.Aw, 11.30.Rd, 12.38.Gc

I. INTRODUCTION

The understanding of the hadron spectrum as well as the phase structure of QCD at finite temperature and density are very important and long-standing problems. Qualitative access to the hadron spectrum beyond low-lying resonances and the phase structure at large densities already requires a quantitative hold on competing fluctuations as well as the phenomena of dynamical chiral symmetry breaking and confinement.

Building on previous studies [1,2], this work, together with a related qualitative study of the unquenched system in [3], provides the foundation for achieving this goal. The present work and [3] are the first works within a collaboration (fQCD) aiming at a quantitative functional renormalization group framework for QCD [4]. While the correct implementation of relative fluctuation scales is not required to reproduce the thermodynamic properties of QCD at vanishing chemical potential [5], it will become increasingly important at finite chemical potential. As was detailed in [6] in the example of quantum/thermal and density fluctuations, mismatches in thermal/density fluctuation scales inevitably lead to large systematic errors at finite chemical potential. This is particularly important for the question of the potential critical end point in the QCD phase diagram.

Functional continuum approaches provide access to the mechanisms of dynamical chiral symmetry breaking and confinement, as well as their interrelation. Up until now, functional computations have required larger or smaller amounts of phenomenological input in the form of running couplings, vertex models, or further low-energy parameters; see [7–18] and references therein. In this work, we present the first closed, self-consistent and quantitative computation for quenched continuum QCD in the vacuum. A prominent feature of this calculation is the lack of additional model input; the computation depends only on the fundamental parameters of QCD, the strong coupling α_s and the current quark masses which are set at a large, perturbative momentum scale. We implement a systematic vertex expansion scheme that is fully capable of taking the nonperturbative physics at low momenta into account. Gauge invariance is implemented and tested in the form of modified Slavnov-Taylor identities (mSTIs). In the present work, we focus on the matter system as one of the two subsectors of the full calculation. Using results for the Yang-Mills propagators [15,19], we solve the matter sector in a quenched approximation and assess the quality of our results in comparison to lattice QCD; see Fig. 1. A separate analysis of the fully coupled system is presented elsewhere.

The paper is organized as follows. In Sec. II we describe our approach to QCD; in particular, we briefly introduce the dynamical hadronization procedure within the functional renormalization group approach and describe the used truncation scheme. In Sec. III, we present our results and comment on the mechanism of chiral symmetry breaking in light of our investigations. Technical details on modified Slavnov-Taylor identities and on our truncation can be found in the Appendixes.

II. QCD WITH THE FUNCTIONAL RG

In quenched QCD there are no matter contributions to the gluon/ghost correlation functions, since these contributions involve only diagrams with closed quark loops. Therefore, all gluon/ghost correlation functions are given by those of the pure Yang-Mills theory. Consequently, we use the functional renormalization group (FRG) results for Yang-Mills gluon and ghost propagators, [15,19] in our calculation.

We perform a vertex expansion including a fully momentum-dependent quark propagator and quark-gluon vertex as well as dynamically generated four-Fermi

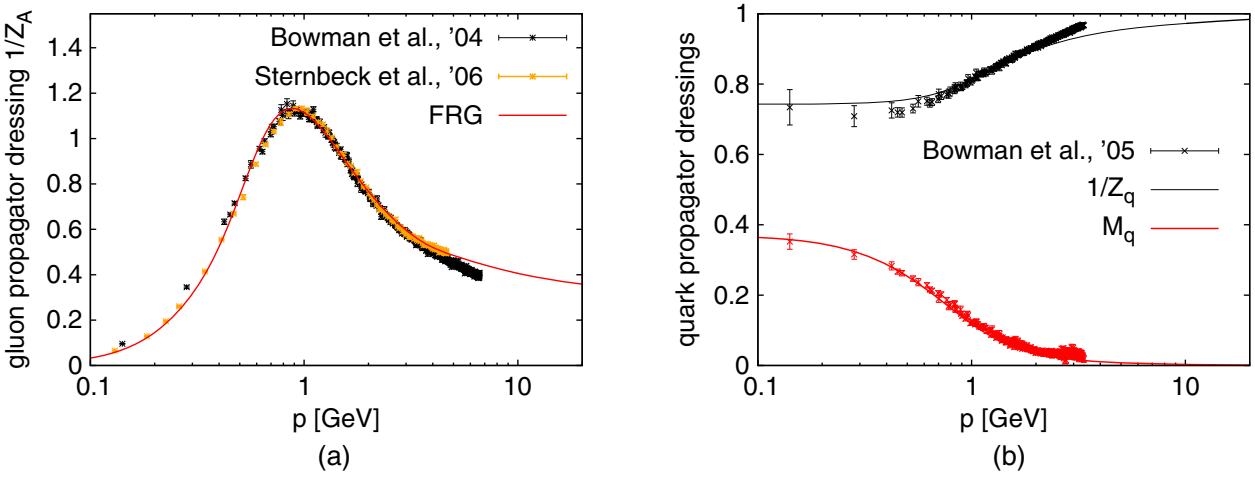

FIG. 1 (color online). FRG results in comparison to lattice QCD. Dimensionful quantities in Bowman *et al.*, [20,21], are rescaled by a factor 0.91 in both plots to match the scales of Sternbeck *et al.*, [22] and the FRG results, [15,19]. (a) Yang-Mills FRG gluon dressing function, (B1), taken from [15,19] in comparison to quenched lattice data [20,22]. (b) Our result for quark propagator dressing functions, (B6), in comparison to quenched lattice results [21] and mass function in GeV.

interactions in the matter sector and ghost-gluon and three-gluon vertices in the glue sector. Furthermore, we use gauge invariance in the form of mSTIs to include higher quark-gluon interactions as well as the four-gluon vertex. Mesonic interactions are included via the mechanism of dynamical hadronization, an RG-scale dependent change of variables which constitutes an economic way to take into account resonant structures in four-Fermi interaction channels. In the following two subsections, we give a brief account of the FRG approach and our truncation scheme. A more complete description of the truncation and a discussion of its stability is found in Appendixes B and C.

A. Dynamical hadronization in the functional renormalization group

The central object in the functional renormalization group approach to quantum field theory is the scale-dependent effective action Γ_k. It generalizes the effective action Γ, in the spirit of the Wilsonian RG, by introducing a cutoff scale k such that Γ_k includes only fluctuations from momentum modes with momenta larger than k; see [7–11] for QCD-related reviews. On a technical level, this is achieved by giving a momentum-dependent mass to modes with momenta smaller than the scale k by means of an infrared regulator function R_k. In this way the scale-dependent effective action Γ_k interpolates between a microscopic action, parametrized by a finite set of parameters, at some large cutoff scale $k = \Lambda_{\mathrm{UV}}$ and the full quantum effective action in the limit $k \to 0$. The evolution of Γ_k with the RG-scale k is described in terms of an exact equation of one-loop structure, [23]

$$\partial_t \Gamma_k = \frac{1}{2}\mathrm{Tr}\frac{1}{\Gamma_k^{(2)} + R_k}\partial_t R_k. \tag{1}$$

Here $\Gamma_k^{(2)}$ denotes the second functional derivative with respect to the fields, $t = \log(k/\Lambda)$ with some reference scale Λ, and the trace includes a sum over all field species and internal indices as well as a momentum-space integration. Note that the flow equation (1) is one-loop exact, higher loop corrections and nonperturbative effects are incorporated due the presence of dressed, field-dependent propagators $(\Gamma_k^{(2)} + R_k)^{-1}$. Flow equations for propagators or higher-order n-point functions are obtained by taking appropriate functional derivatives of (1). Despite its nature as an exact equation, most practical applications require an ansatz for the scale-dependent effective action. Therefore, identifying the operators that carry the relevant physical information is of utmost importance for any quantitatively reliable solution of the flow equation (1).

Four-Fermi interactions, e.g. in the scalar channel with coupling $\lambda_{(\bar{\psi}\psi)^2}$, are created dynamically from two-gluon exchange box diagrams that are proportional to α_s^2. The back-coupling of these four-Fermi interactions on the system is suppressed by additional powers of α_s^2, for example its contributions to the four-Fermi system is of order α_s^4. However, as the strong running coupling, α_s, becomes large close to Λ_{QCD}, the suppression of the four-Fermi interactions is overcome and they start to grow large. As it becomes sufficiently large, the four-Fermi dynamics eventually become dominant and lead to a four-Fermi resonance. This resonance corresponds to the light pions as pseudo–Nambu-Goldstone modes in the spontaneously broken phase. For even smaller momentum scales, quark interactions exhibit dominant scatterings of these resonant momentum channels. Hence, it is advantageous to describe these interactions in terms of composite operators, which is achieved via the introduction of scale-dependent mesonic field operators [3,8,24,25]. In the present work, we follow

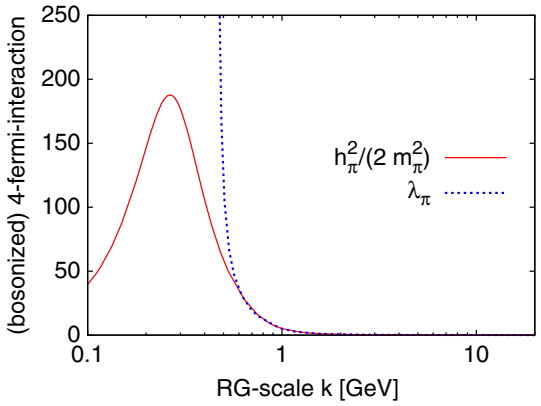

FIG. 2 (color online). Dynamical hadronization: four-Fermi coupling (λ_π, see Appendix B 2 c) vs corresponding coupling from dynamical hadronization, $(kh_\pi)^2/(2m_\pi^2)$, in a momentum-independent approximation similar to [3].

the dynamical hadronization procedure set up in [3,8]. In each renormalization group step this leads e.g. to $\lambda_\pi \to h_\pi^2/(2m_\pi^2)$ at vanishing s-channel momentum in the four-Fermi channel. Here λ_π corresponds to the exchange of pions with mass m_π and Yukawa coupling h_π. This exact dynamical change of field-variables avoids the numerically inconvenient singularity shown in Fig. 2, which is a consequence of neglected momentum dependencies in the four-Fermi interaction. Additionally, it provides a smooth transition from QCD degrees of freedom to constituent quarks and light mesons as low-energy effective degrees of freedom. The resulting low-energy description in terms of a quark-meson model introduces no model parameter dependence provided the UV initial scale is chosen large enough $\Lambda_{\mathrm{UV}} \gg \Lambda_{\mathrm{QCD}}$; see Sec. III D for an explicit demonstration. Finally we want to stress that the restriction to such a small set of low-energy degrees of freedom is justified by the comparably large masses in the remainder of the spectrum of the strong interaction. Since any of the hadrons can play a dynamical role only below about 500 MeV, their fluctuations are strongly suppressed in any of the loops by their comparably large mass; see also [3].

B. Truncation of effective action

In our truncation we consider the momentum dependence of all vertices which include at least one relevant or marginally relevant operator with the help of [26]. In the pure glue sector we calculate the ghost- and three-gluon vertices in single channel approximations including only the classical tensor structure. Moreover we use modified Slavnov-Taylor identities to fix the momentum dependence of the four-gluon vertex in this channel. This approximation is motivated by results from other methods [30–35], which show nontrivial momentum dependencies only in momentum regions where the gluon sector already starts to decouple from the system. The matter-glue coupling as the interface between the two subsectors of the system is of crucial importance for the whole system. Therefore, we include the full momentum dependence and all eight tensor structures in the quark-gluon vertex. Furthermore, there are two exceptions from the RG relevance counting, in the sense that we also include perturbatively irrelevant operators in our truncation. Firstly, in the matter sector we include in addition the four-Fermi interactions, which are required for the description of chiral symmetry breaking. Secondly, for any nonclassical operator which shows a significant contribution in the flow, we identify the corresponding gauge-invariant completion and include the resulting higher-order vertices in the flow equations.

The general vertex construction follows [36]. Suppressing the explicit RG-scale dependence we parametrize

$$\Gamma^{(n)}_{\Phi_1\cdots\Phi_n}(p_1,\ldots,p_{n-1}) = \bar{\Gamma}^{(n)}_{\Phi_1\cdots\Phi_n}(p_1,\ldots,p_{n-1})\prod_{i=1}^{n}\sqrt{\bar{Z}_{\Phi_i}(p_i)}, \tag{2}$$

where we introduced a superfield

$$\Phi = (A_\mu, c, \bar{c}, q, \bar{q}, \vec{\pi}, \sigma, \ldots) \tag{3}$$

which subsums all dynamical degrees of freedom including the effective low-energy fields generated by dynamical hadronization. The tensor kernel $\bar{\Gamma}^{(n)}_{\Phi_1\cdots\Phi_n}$ is expanded in a basis of tensor structures $\mathcal{T}^{(i)}_{\Phi_1\cdots\Phi_n}$

$$\bar{\Gamma}^{(n)}_{\Phi_1\cdots\Phi_n}(p_1,\ldots,p_{n-1}) = \sum_i z^{(i)}_{\Phi_1\cdots\Phi_n}(p_1,\ldots,p_{n-1})\mathcal{T}^{(i)}_{\Phi_1\cdots\Phi_n}(p_1,\ldots,p_{n-1}). \tag{4}$$

Since the dressing functions $z^{(i)}_{\Phi_1\cdots\Phi_n}(p_1,\ldots,p_{n-1})$ depend on our choice of $\bar{Z}_{\Phi_i}$, the latter are at our disposal to give special properties like RG-invariance in the perturbative regime to the former. If not specified otherwise, we choose $\bar{Z}_{\Phi_i}(p) \equiv Z_{\Phi_i,k}(p)$, where the $Z_{\Phi_i,k}(p)$ are the scalar dressing functions of the full propagators; see Appendix B. An important example are the classical vertices with tensor structures $\mathcal{T}_{\mathrm{class}}$ present in the classical action. We use

$$\mathcal{T}_{\mathrm{class},\Phi_1\cdots\Phi_n}(p_1,\ldots,p_{n-1}) = S^{(n)}_{\Phi_1\ldots\Phi_n}|_{g=1}, \tag{5}$$

where $S^{(n)}$ denotes the appropriate n-th functional derivative of the action. By setting $g=1$ in (5), the running coupling is taken into account via the dressing functions $z^{(1)}_{\Phi_1\cdots\Phi_n}$ in (4). As a consequence of our choice for $\bar{Z}_{\Phi_i}(p)$, the $z^{(1)}_{\Phi_1\ldots\Phi_n,k\equiv 0}(p_1,\ldots,p_{n-1})$ run like appropriate powers of

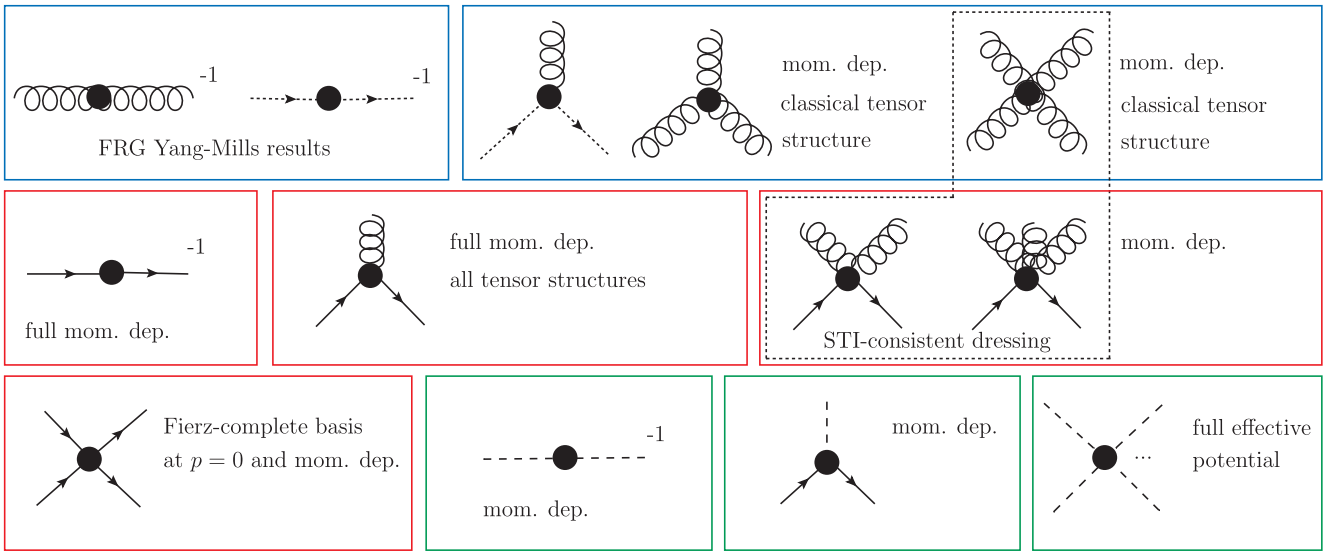

FIG. 3 (color online). Pictorial description of our truncation for the effective action; see Fig. 7 for corresponding RG flows.

the strong running coupling with the momenta p_i in the perturbative regime. The same holds for the RG-scale dependence of the $z^{(1)}_{\Phi_1\ldots\Phi_n}(0,\ldots,0)$ at perturbative scales.

In the following we discuss in some detail the constituents of our ansatz for the bosonized effective action of Landau-gauge QCD, which are also summarized pictorially in Fig. 3. For a more detailed description the reader is referred to Appendix B. The stability of this truncation and the systematic errors are discussed in Appendix C.

Glue sector: As a consistent scale-setting both in the perturbative and in the nonperturbative regime is crucial for our calculation, we use YM FRG data [15,19] for both the gluon propagator and the ghost propagator; see Fig. 1(a). Here, we have matched our scale to the corresponding lattice scales in [22] via the peak position in the gluon dressing function $1/Z_A$, which translates to

$$\alpha_s(20\ \mathrm{GeV}) = 0.21. \tag{6}$$

The dressing functions of the Yang-Mills three-point functions, $z_{\bar{c}Ac}$, z_{A^3}, are calculated momentum dependently for a single momentum channel. The four-gluon vertex is approximated using the three-gluon vertex; see Appendix B 1 b. This is a very good approximation down to semi-perturbative momenta [30–35], whereas deviations occur mostly for momenta where the glue gap implies already decoupling.

Matter sector: We take into account the full momentum dependence of the quark propagator, parametrized by its wave function renormalization $Z_q(p)$ and mass function $M_q(p)$, where we have for the current quark mass

$$M_q(20\ \mathrm{GeV}) = 1.3\ \mathrm{MeV}, \tag{7}$$

(see Appendix B 2 a for details). The treatment of the quark-gluon vertex is of crucial importance for the whole system. Therefore, we include the full momentum dependence of all eight linearly independent tensor structures $\mathcal{T}^{(i)}_{\bar{q}Aq}$ of Landau gauge as described in Appendix B 2 b. Additionally we perform a gauge-invariant completion of any quark-gluon vertex tensor structure that contributes quantitatively, leading to the inclusion of two-quark–two-gluon and two-quark–three-gluon vertices that are approximated gauge invariantly; see Appendix B 2 b.

In the four-Fermi sector, we take into account a Fierz-complete basis of all ten tensor structures consistent with a $U(1)_V \times SU(2)_V$ symmetry (see Appendix B 2 c) and approximate their momentum dependence using a single (s-channel) momentum variable. As discussed previously, we utilize dynamical hadronization to effectively remove the resonant $\sigma - \pi$ channel from the four-Fermi tensor structures via the inclusion of effective (quark-)meson interactions.

In the mesonic sector we include a scale-dependent mesonic wave function renormalization factor, Z_π, and a Yukawa interaction between quarks and mesons, h_π. Additionally, a scale-dependent effective potential, $U(\rho)$ captures higher mesonic interactions in the nonperturbative regime of spontaneously broken chiral symmetry; see e.g. [37]. This approximation has been shown to be in quantitative agreement with the full momentum dependence [6].

III. RESULTS

A. Quark-gluon interactions

We start by considering the quark-gluon vertex and focus in particular on additional nonclassical tensor structures, as

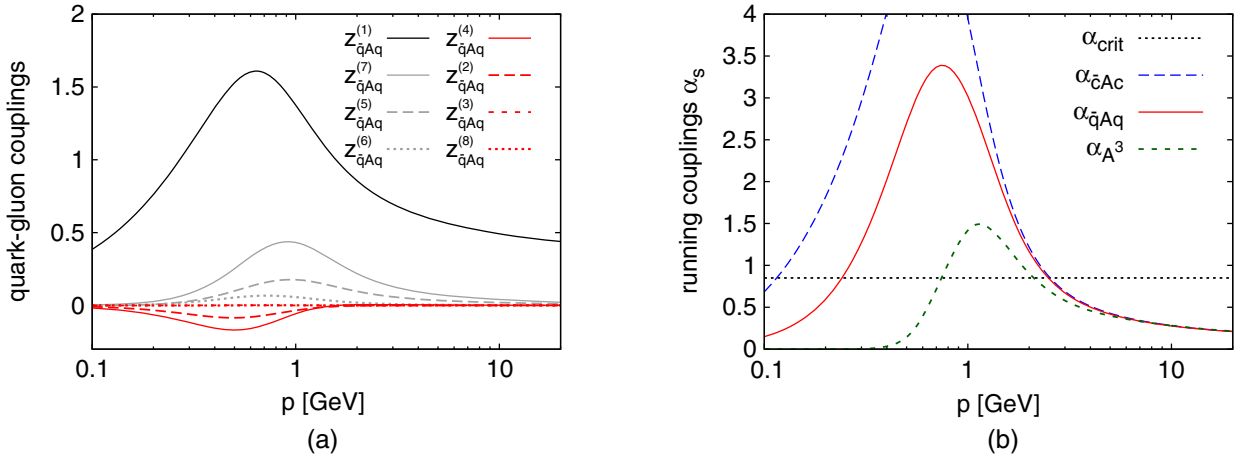

FIG. 4 (color online). Strength of tensor structures and vertices. (a) Coupling strength, (17) and (B9), of quark-gluon vertex tensor components at symmetric point. Black: classical tensor structure, grey: chirally symmetric non-classical tensor structures, red: tensor structures that break chiral symmetry. (b) Running couplings α_s at symmetric point $p_1^2 = p_2^2 = (p_1 + p_2)^2$ from different vertices which takes the gluon gap into account analogous to (17) for the quark-gluon vertex. Critical gauge coupling for chiral symmetry breaking α_{crit}.

they are shown for the symmetric momentum configuration $p_1^2 = p_2^2 = p_3^2$ in Fig. 4(a). To investigate their importance we calculate the full momentum dependence of a basis for the transversally projected Landau-gauge quark-gluon vertex. The resulting eight tensor structures include the classical tensor structure,

$$[T^{(1)}_{\bar{q}Aq}]^\mu = \gamma^\mu, \tag{8}$$

three further chirally symmetric tensors

$$T^{(5)}_{\bar{q}Aq}, \qquad T^{(6)}_{\bar{q}Aq}, \qquad T^{(7)}_{\bar{q}Aq}, \tag{9}$$

and four tensors which break chiral symmetry

$$T^{(2)}_{\bar{q}Aq}, \qquad T^{(3)}_{\bar{q}Aq}, \qquad T^{(4)}_{\bar{q}Aq}, \qquad T^{(8)}_{\bar{q}Aq}, \tag{10}$$

listed explicitly in Appendix B 2 b. Each of the eight tensor structures leads to a contribution in the effective action that, if separated from the remainder of the action, violates gauge invariance. For example, the classical tensor structure, γ^μ, corresponds to the term $\bar{q}\not{A}q$ in the effective action which is by itself not gauge invariant. However, it appears as part of the gauge-covariant derivative $\bar{q}\not{D}q$ which respects gauge invariance. On the other hand, for the additional tensor structures, $T^{(i)}_{\bar{q}Aq}$, $i > 1$, such a gauge-covariant completion is not automatically included. A naïve inclusion of these tensor structures alone would, therefore, violate gauge invariance in the form of (modified) Slavnov-Taylor identities; see the discussion in Appendix A.

In the semi-perturbative, chirally symmetric regime we find the gauge-invariant operator

$$\mathrm{i}\sqrt{4\pi\alpha_s}\bar{q}\gamma_5\gamma_\mu\epsilon_{\mu\nu\rho\sigma}\{F_{\nu\rho}, D_\sigma\}q, \tag{11}$$

whose contribution to the term of $\mathcal{O}(\bar{q}Aq)$ is proportional to the tensor

$$\frac{1}{2}T^{(5)}_{\bar{q}Aq} + T^{(7)}_{\bar{q}Aq}. \tag{12}$$

Together with our results for the dressing functions, $z^{(i)}_{\bar{q}Aq}(p,q)$ evaluated at $p^2 = q^2 = (p+q)^2$, Fig. 4(a), we conclude that this is indeed the gauge-invariant operator that determines most of the strength of the chirally symmetric nonclassical tensor structures; see also Fig. 6. Since the operator in (11) contributes also to tensor structures in higher vertices, namely the two-quark–two-gluon and two-quark–three-gluon interactions, we include these as well in our truncation and dress them in accordance with gauge symmetry, see Appendixes A 2 and B 2 b for further details. Similarly we find that the chiral symmetry breaking operator

$$\bar{q}(\delta_{\mu\nu} + [\gamma_\mu, \gamma_\nu])D_\mu D_\nu q, \tag{13}$$

contributes to $\mathcal{O}(\bar{q}Aq)$ to the tensor

$$\frac{1}{2}T^{(2)}_{\bar{q}Aq} + T^{(4)}_{\bar{q}Aq}. \tag{14}$$

Since this is the most relevant operator in the phase of spontaneously broken chiral symmetry we again include the corresponding contribution to the two-quark—two-gluon vertex with gauge invariant dressing. The explicit calculation of the dressing functions of the higher interactions to check the quantitative importance of deviations from the STI which are expected to occur below momenta of $\mathcal{O}(1\ \text{GeV})$ is deferred to future work.

We want to stress at this point that if we would only take into account a full basis for the quark-gluon vertex without the corresponding gauge invariant partner tensor structures in the higher vertices, we would see considerably different results. In particular, the running coupling (see Fig. 4), as

defined from the dressing function of the classical tensor structure, $z^{(1)}_{\bar{q}Aq}$, would deviate from the corresponding ghost-gluon running coupling at considerably larger momenta. However, the degeneracy of the running couplings defined from the different vertices at semi-perturbative momentum scales is a consequence of gauge invariance. Hence we conclude that the higher quark-gluon vertices are important for the consistency of the truncation. Moreover, diagrams that contain the two-quark–two-gluon vertex have a different number of quark lines than the ones that contain only classical vertices. Consequently, the balance between diagrams with classical and nonclassical vertices is changed by a finite chemical potential.

Note that for assessing the importance of the different tensor structures one has to take into account not only their relative strength but also their respective symmetry properties. For example, simply extracting the relative strength from Fig. 4(a), we would conclude that the operator in (11) seems to be the most important one by far. We find, however, that also the operator in (13) is very important for the value of the quark propagator mass function. This is explained by the fact that (13) breaks chiral symmetry and contributes, therefore, directly to the quark mass function.

B. Quark propagator

Next we discuss our solution for the quark propagator parametrized as

$$\Gamma_{\bar{q}q}(p) = Z_q(p)(\mathrm{i}\not{p} + M_q(p)), \tag{15}$$

which is shown in Fig. 1(b); for an earlier study, see e.g. [38]. Particular focus will be put on the effect of different quark-gluon interactions. We find very convincing agreement with results obtained in lattice QCD in the quenched approximation [21], that are shown with dimensionful quantities rescaled by a factor of 0.91 to match the scale of [22] and [15,19]. However, some care is necessary when comparing our propagator to the lattice results, since the quenched approximation in lattice simulations sets the fermion determinant to unity, whereas we just used a quenched gluon propagator.

Apart from the classical tensor structure, the most important contribution to the quark propagator stems from the tensor structures $\frac{1}{2}\mathcal{T}^{(5)}_{\bar{q}Aq} + \mathcal{T}^{(7)}_{\bar{q}Aq}$ for $Z_q(p)$, and $\frac{1}{2}\mathcal{T}^{(2)}_{\bar{q}Aq} + \mathcal{T}^{(4)}_{\bar{q}Aq}$ for $M_q(p)$, where we find it necessary to include the full momentum dependence of the corresponding dressing functions $z^{(i)}_{\bar{q}Aq}(p,q)$. It is only the combination of all these terms, including their gauge invariant partner structures in the quark-gluon vertex equation together with their momentum dependencies, that leads to the very good agreement with the lattice propagator. In particular this concerns the wave function renormalization $Z_q(p)$ for small momenta, where an important contribution stems from mesonic fluctuations in the infrared. These fluctuations have been included with functional methods, e.g. in [2,7,39–45]. Restricting the discussion only to the relative importance of quark-gluon vertex tensor structures, recent findings in Dyson-Schwinger studies [46–48] agree with ours; see also [49] for an earlier study. Moreover, our present findings suggest the inclusion of the STI-consistent higher quark-gluon interactions in future DSE-studies.

Finally we want to point out that one crucial contribution to the quark mass function comes from the addition to the flow of the Yukawa coupling, $\partial_t \Delta h$, due to dynamical hadronization; see (D7). As soon as one runs into the spontaneously broken phase of QCD, $\langle\sigma\rangle \neq 0$, this term contributes to the quark mass function as well via the relation $\partial_t \Delta M_q(0) \propto \langle\sigma\rangle \partial_t \Delta h_\pi$. Momentum dependencies are very important in $\partial_t \Delta M_q(p)$, since we expect this term to be approximately zero for momenta larger than the chiral symmetry breaking scale; see Appendix D for details. Similarly, we had to include momentum dependencies in the remaining four-Fermi interactions that appear in the tadpole diagram. In the language of dynamical hadronization, chiral symmetry breaking in terms of the quark mass function is then triggered by the additional term, $\partial_t \Delta M_q$; see (D9). This, however, is just due to the chosen parametrization of the four-Fermi interaction in terms of mesons. Without dynamical hadronization, chiral symmetry breaking would be driven by the tadpole diagrams containing the resonant (momentum-dependent) four-Fermi channel, which in turn is driven by quark-gluon interactions.

C. Gluonic vertices and running couplings

From our calculated momentum-dependent QCD vertices, namely from the quark-gluon, the ghost-gluon and the three-gluon vertex we can extract running couplings. Following the detailed discussion in Appendix A, these running couplings are required to be degenerate at (semi-) perturbative momenta $p \gtrsim \mathcal{O}(1\ \mathrm{GeV})$ by means of Slavnov-Taylor identities,

$$4\pi\alpha_S(p) = z^2_{\bar{c}Ac}(p) = z^2_{\bar{q}Aq}(p) = z^2_{A^3}(p) = z_{A^4}(p), \tag{16}$$

whereas they will start to deviate in the nonperturbative regime $p \lesssim \mathcal{O}(1\ \mathrm{GeV})$. Additionally, there is no unique definition of a running coupling extracted from a particular vertex in the nonperturbative regime. Here we define effective running couplings that explicitly take the decoupling due to the gluonic mass gap into account, illustrated exemplarily for the running coupling extracted from the quark-gluon vertex evaluated at the symmetric point,

$$\alpha_{\bar{q}Aq}(p^2) = \left.\frac{\left(z^{(1)}_{\bar{q}Aq}(p,q)\right)^2}{4\pi}\right|_{p^2=q^2=(p+q)^2}. \tag{17}$$

The running couplings from different vertices are shown in Fig. 4. Irrespective of the definition, all running couplings

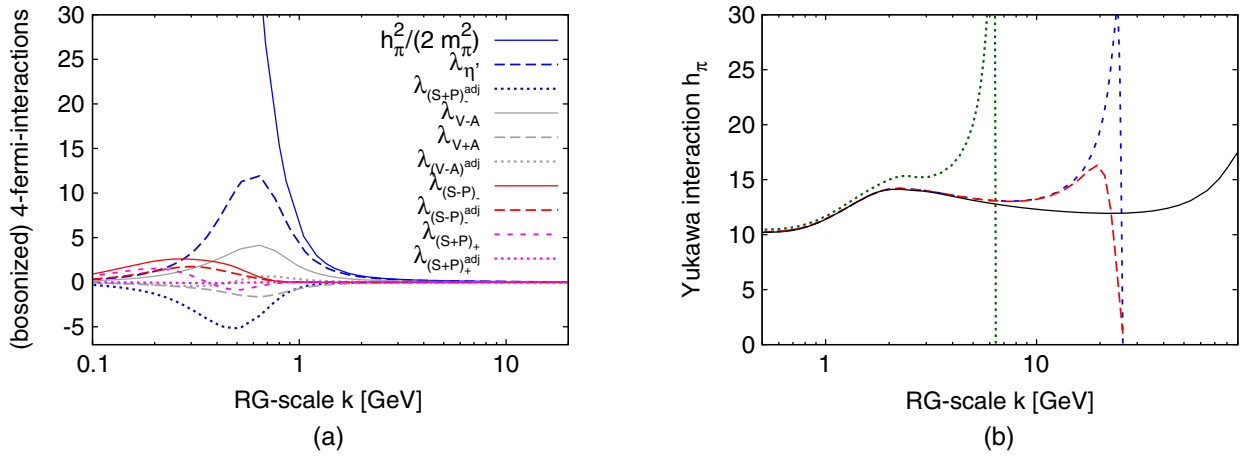

FIG. 5 (color online). RG-scale dependence of four-Fermi interactions and Yukawa coupling. (a) Renormalisation group scale dependence of dimensionless four- fermi interactions, see Appendix B 2 c, and bosonised σ-π channel. Grey: respects chiral symmetry, blue: breaks $U(1)_A$, red: breaks $SU(2)_A$, magenta: breaks $U(2)_A$. (b) Independence of infrared model parameters from initial value and scale demonstrated for Yukawa coupling in a momentum-independent approximation similar to [3].

coincide down to momenta of 4 GeV. This underlines the fact that STI violations are negligible, without the necessity to tune initial conditions as an implicit solution of the STI as described in Appendix A 1. Even more, the degeneracy of all running couplings at large momenta represents a highly nontrivial statement about the consistency of our truncation, in the sense that all important contributions in the semi-perturbative regime have been consistently taken into account. Note that the very good agreement of the quark-gluon and the ghost-gluon running coupling is in part a consequence of the full momentum dependence which is self-consistently taken into account in the quark gluon vertex. This suggests that a similar improvement in the glue sector might lead to an even better agreement of the three-gluon coupling with the two other couplings. At low momenta, the gap in the gluon propagator becomes important and we find a clear difference between the strength of the various vertices. In particular, the three-gluon vertex drops considerably earlier, which is mainly due to the larger number of gluon legs.

D. Relative importance of four-Fermi channels

As mentioned in the discussion of our truncation in Sec. II B, we include a Fierz-complete basis with all ten basis elements consistent with the $SU(N_c)_c \otimes SU(N_f)_V \otimes U(1)_B$ symmetry to assess the importance of different four-Fermi interaction channels; see Appendix B 2 c for details on the choice of the basis. All four-Fermi couplings are shown in Fig. 5(a), where in particular $h_\pi^2/2m_\pi^2$ corresponds to the dressing function of the tensor structure

$$(\bar{q}T^0 q)^2 - (\bar{q}\gamma^5 T^f q)^2, \tag{18}$$

and $\lambda_{\eta'}$ to the dressing function of

$$(\bar{q}T^f q)^2 - (\bar{q}\gamma^5 T^0 q)^2, \tag{19}$$

where T^f (T^0) denote the generators of $SU(N_f)$ ($U(1)$). We find that the dynamics of spontaneous chiral symmetry breaking is almost exclusively driven by the chirally symmetric four-Fermi channel $\lambda_{(S-P)_+}$, which corresponds to the quantum numbers of the σ, π, η and a mesons. However, this channel is split by the presence of the 't Hooft determinant coupling, $\lambda_{(S+P)_-}$, such that only the σ meson and pions become very light. The dynamically created quark mass is already sufficient to strongly suppress the η' channel in comparison to the resonant pion channel. Additional contributions due to the $U(1)_A$ anomaly would lead to an even stronger suppression; see [41,50]. Additionally, for sufficiently large initial scales, these anomalous contributions are suppressed relative to the contribution that orginates from the explicit symmetry breaking due to nonvanishing current quark masses. First checks indeed indicate that the anomalous contributions at a sufficiently initial large cutoff scale do not play a quantitatively important rôle, a more detailed study will be presented elsewhere. On the other hand, anomalous contributions corresponding to fluctuations below the cut-off scale are already taken into account by integrating the FRG running. This has also been demonstrated e.g. for the quantum mechanical anharmonic oscillator [51]. Therefore, all but the resonant pion four-Fermi channel constitute subleading contributions with a quantitative effect of less than 5%; see Fig. 2. Independent of their relative strength, the suppression of any of the four-Fermi interactions is overcome by the strength of α_s only in the nonperturbative regime of QCD at scales of $\mathcal{O}(1\ \mathrm{GeV})$.

In light of these results it is sufficient to take into account only the $(\sigma - \pi)$ channel, provided one uses a projection obtained from a full basis to avoid ambiguities in the

projection procedure. Furthermore, note that in the purely fermionic theory all ten channels diverge at the chiral symmetry breaking scale signaling resonant quark-anti-quark states, as illustrated in Fig. 2 for the $(\sigma-\pi)$ channel. These divergencies are a consequence of ignoring momentum dependencies and can be removed by dynamically hadronizing only the $(\sigma-\pi)$ channel. Nevertheless, it would be interesting to also bosonize other four-Fermi channels to investigate the properties of the corresponding bound states. Alternatively an investigation of the momentum dependencies of the four-Fermi interactions themselves is also conceivable. As a word of caution, our statements about the relative strength of four-Fermi channels are only valid in the vacuum as in particular finite chemical potential is expected to shift the relative strength of four-Fermi interaction channels. This expectation is based on the picture that different effective degrees of freedom like diquarks might become important at larger chemical potentials which would manifest itself also in the corresponding 4-Fermi interaction channels.

Finally we want to mention that Fig. 5(a) captures only the zero external momentum limit of the four-Fermi interaction channels. Although it was necessary to calculate the momentum dependence of the s-channel momentum configuration for the evaluation of the quark-propagator for this work, we postpone a thorough discussion of the momentum dependence of the four-Fermi interactions to future publications. Here we only note that the effect of such momentum dependencies on the remainder of the matter system is very weak, since all but the σ-π channel are very weak. In the latter, on the other hand, we have implicitly taken momentum dependencies into account via dynamical hadronization.

Furthermore, we want to stress that the dynamical hadronization procedure of introducing effective mesonic degrees of freedom introduces no model parameters in the theory. Therefore, the infrared physics in terms of quarks and mesons is independent of the ultraviolet starting point and initial values. This is demonstrated explicitly for the Yukawa interaction between quarks and mesons in Fig. 5(b). The flow of the four-Fermi channel λ_π determines only the value of the ratio $h_\pi^2/(2m_\pi^2)$, which rises monotonously in the perturbative regime, cf. Fig. 5(a). Although the inital flows of the Yukawa coupling h_π and pion mass m_π^2 depend on their particular inital values, each pair of initial values $(h_{\pi,\Lambda}, m^2_{\pi,\Lambda})$ at any reasonably large UV-scale Λ leads to the same infrared values. As is demonstrated in Fig. 5(b), the flows of, e.g. the Yukawa coupling with different initial values and/or scales, converge to the same infrared value after a short tuning phase.

E. Mechanism of chiral symmetry breaking

As outlined in the introduction a proper understanding of the mechanisms of confinement and chiral symmetry breaking is a crucial step towards a quantitatively reliable approach to the phase diagram of QCD at finite chemical potential. Here we comment on the mechanism of chiral symmetry breaking from the point of view of the matter system.

In [11,24,52–56] a simple picture for chiral symmetry breaking in quenched QCD was put forward. In their analysis the IR fixed points in the four-Fermi interactions are destabilized if the gauge coupling exceeds a critical coupling $\alpha_{\rm crit}$ and as a result the four-Fermi coupling becomes singular. Although the argument is qualitatively correct, in quenched QCD the picture is not so simple, as the drop of the gauge coupling at small momenta [see Fig. 4(b)], lets the quark sector become subcritical again. This was discussed as one possible scenario in [56], but is confirmed here as the actual physical situation. In Fig. 4(b), we show the different running couplings and the critical gauge coupling. Since the gauge coupling decreases below the critical coupling for decreasing momenta, it is merely the area above the critical value line which is decisive for the occurrence of chiral symmetry breaking.

Our findings indicate that an approach where the vertex strength of all tensor structures of the quark-gluon vertex is subsummed in an enhanced strength of the classical tensor structure lacks quantitative precision. Using such an enhanced quark-gluon vertex in our calculation would lead to much too large contributions in the four-Fermi sector, from gluonic box diagrams which grow like $\alpha^2_{\bar{q}Aq}$. Taking into account different tensor structures approximately corresponds to a sum of contributions $\simeq\sum_i\alpha_i^2$, if we denote the running couplings associated to different components of the quark-gluon vertex as α_i and neglect cross terms, whereas the enhanced vertex from the single channel approximation contributes as the square of the sums $\simeq(\sum_i\alpha_i)^2$ in the four-Fermi box diagram.

Finally, we briefly discuss the mechanism of chiral symmetry breaking which is at work in our framework. Here, chiral symmetry breaking is driven by four-Fermi interactions. In a framework of dynamical hadronization this is reflected in the corresponding contributions to the Yukawa coupling/quark mass. Therefore, our calculation requires significantly less vertex strength in the quark-gluon vertex in order to see chiral symmetry breaking compared to the required strength in single channel approximation as described above. In our framework, including just the classical tensor structure in the quark-gluon vertex leads to qualitatively albeit not quantitatively correct results. This is mainly due to the contributions from the tensor structure $\frac{1}{2}\mathcal{T}^{(5)}_{\bar{q}Aq}+\mathcal{T}^{(7)}_{\bar{q}Aq}$ in the quark-gluon vertex and its gauge invariant completion; see the discussion in Sec. III A and Appendix B 2.

IV. SUMMARY AND CONCLUSIONS

In the present work, we have investigated spontaneous chiral symmetry breaking in quenched continuum QCD. The only relevant couplings are those of QCD: the strong

coupling α_s and the current quark masses which are fixed in the perturbative regime. In particular, this allows us to compute the quark propagator in excellent agreement with corresponding results from lattice QCD.

The functional renormalization group analysis presented here uses a vertex expansion that goes qualitatively beyond the approximation level used so far in continuum methods. On the one hand, advanced approximations have been used in subsystems such as the pure glue sector and the low-energy matter sector. On the other hand, we have, for the first time, introduced a complete basis of four-Fermi interactions in the s channel as well as the full quark-gluon vertex with all its momentum dependencies and tensor structures. The latter has been linked to higher-order quark-gluon interactions via modified Slavnov-Taylor identities. These higher-order terms are also important for the convergence of the results, which emphasizes the necessity of an expansion scheme based on gauge-invariant operators. The quantitative reliability has been discussed in a detailed analysis of the systematic errors.

The transition from the quark-gluon to the hadronic phase is smoothly done by means of dynamical hadronization. This allows us to monitor the emergence of composite mesonic operators as dynamical degrees of freedom at low energies. We have also investigated the relative importance of different four-Fermi interaction channels. Here we find that a single channel approximation with σ and $\vec{\pi}$ is sufficient to induce spontaneous chiral symmetry breaking on a semi-quantitative level. This fact together with the small width of the strongly correlated transition region from the quark-gluon regime to the hadronic regime (see also [3]) can be used to systematically improve the reliability of low-energy effective models; see [5,57–59].

The present computation is currently being extended to full dynamical QCD (for first investigations, see [3]) and to finite temperature and density. Our analysis of the matter sector should also give access to the large density regime, provided the higher fermionic interactions including fluctuating baryons are monitored accordingly.

ACKNOWLEDGMENTS

We thank R. Alkofer, J. Braun, C. S. Fischer, L. Fister, T. K. Herbst, M. Hopfer, M. Q. Huber, F. Rennecke, B.-J. Schaefer, L. von Smekal, R. Williams and A. Windisch for discussions. This work is supported by the Helmholtz Alliance HA216/EMMI, Grant No. ERC-2011-ADG_20110209, the FWF through Erwin-Schrödinger-Stipendium No. J3507 and the BMBF Grant No. 05P12VHCTG.

APPENDIX A: MODIFIED SLAVNOV-TAYLOR IDENTITIES

In the presence of the regulator terms the standard Slavnov-Taylor identities (STI) are modified (mSTI). Here we briefly discuss these modifications and their implications following [8], a more detailed study will be presented elsewhere. A very concise form of these identities is found in a formulation with the auxiliary Nakanishi-Lautrup field λ with

$$e^{-\frac{1}{2}\int_x(\partial_\mu A^a_\mu)^2} \to \int \mathcal{D}\lambda e^{-\frac{1}{2}\int_x \partial_\mu A^a_\mu \lambda^a - \frac{\xi}{2}\int_x \partial_\mu \lambda^a \lambda^a}, \tag{A1}$$

where the full classical action $S = S_{\rm QCD} + S_{\rm gf} + S_{\rm ghost}$ is invariant under the BRST transformations

$$\mathfrak{s}\Phi = \left(D_\mu c, -\frac{1}{2} f^{abc} c^b c^c, \lambda^a, -cq, \bar{q}c, 0, 0, \ldots\right), \mathfrak{s}\lambda = 0. \tag{A2}$$

with Φ as defined in (3). In (A2) we have assumed that all the composite fields introduced in Φ are colorless. The introduction of the auxiliary field λ leads to $\mathfrak{s}^2\phi = 0$. The cutoff terms are not invariant under the BRST transformations in (A2) and the standard STI is modified. It reads in a compact way [8,60–62]

$$\int \frac{\delta\Gamma_k}{\delta Q_{\phi_i}}\frac{\delta\Gamma_k}{\delta\phi_i} = \int R_{k,\phi_n\phi_i}\frac{\delta^2\Gamma_k}{\delta Q_{\phi_i}\delta\phi_j} G_{\phi_j\phi_n}, \tag{A3}$$

where we have added a BRST source term

$$\int Q_{\phi_i}(\mathfrak{s}\phi)_i, \tag{A4}$$

to the path integral, see [8] for more details and further references. The sums in (A3) run over all species of fields including internal indices.

1. Initial conditions for vertices

In the limit $k \to 0$ the left-hand side of (A3) vanishes and we arrive at the standard STI: the derivative of Γ with respect to Q_ϕ generates the (quantum) BRST transformations that act linearly on the fields via the derivative of Γ with respect to ϕ. For perturbative momenta p this gives the standard relations between the renormalization factors of the vertex functions at $k = 0$, that is

$$z^2_{\bar{c}Ac}(p) = z^2_{\bar{q}Aq}(p) = z^2_{A^3}(p) = z_{A^4}(p), \tag{A5}$$

corresponding to degenerate running couplings in the perturbative regime. Equation (A5) entails that in QCD the parameters of the theory are given by the power-counting relevant mass parameters of the quarks (dimension one), one (marginal) coupling, α_s, and the unobservable (marginal) wave function renormalizations of the fundamental fields.

In turn, for $k \neq 0$ the simple relations in (A5) are in general lost and the loop term on the right-hand side of (A3)

leads to modifications. In terms of power-counting the most relevant modification is the occurrence of a longitudinal gluon mass parameter $m^2_{k,L}$ in the gluon propagator that vanishes for $k \to 0$. Perturbatively it relates to a transversal mass parameter $m^2_{k,\perp,\mathrm{pert}} = m^2_{k,L,\mathrm{pert}}$. Nonperturbatively this relation does not hold anymore, as we have a nonvanishing transversal mass gap in Landau gauge, for more details see [19]. In the present work, we do not solve the mSTIs for the vertices explicitly and also avoid the necessity of discussing the decoupling of transversal and longitudinal parameters. We take the very good realization of (A5) in our results, i.e. Fig. 4, as an indication that the effects of the right-hand side of (A3) at the initial scale Λ are either small or become unimportant during the evolution of flow equation.

2. STI-invariant vertices

In the perturbative regime, the relations between the gluonic vertices can be obtained with the help of the renormalization group invariant covariant derivative

$$D_\mu = \partial_\mu - i\sqrt{4\pi\alpha_s \bar{Z}_A} A_\mu, \tag{A6}$$

with the renormalized gauge field A_μ. Using the corresponding field strength tensor

$$F_{\mu\nu} = \frac{i}{\sqrt{4\pi\alpha_s}}[D_\mu, D_\nu], \tag{A7}$$

in the effective action leads to gluonic vertices that are consistent with gauge invariance for momenta $p \approx k$ down to $\mathcal{O}(1\ \mathrm{GeV})$. By using $\alpha_{s,k}(p)$ and $Z_{A,k}(p)$ these relations could be made true for a larger range of momenta, which, however, is not necessary due to the locality of the flow. In any case, such relation cannot be found for the nonperturbative regime, since the perturbative mSTIs are in general only valid for the longitudinal part of the vertices which deviate from their transversal parts at nonperturbative momenta as it is for example the case for the gluon mass gap. Consequently, the vertices have to be computed separately and do not follow from the mSTI at low momenta. However, the gluonic vertices and ghost-gluon vertex gain a potentially significant nontrivial momentum dependence and nonclassical tensor structures only in the deep infrared where their contributions decouple due to the mass gap in the gluon propagator. In the present work, we use this as a justification for approximating the four-gluon vertex by the three-gluon vertex.

On the other hand, the quark-gluon vertex potentially gets a significant nontrivial momentum dependence and nonclassical tensor structures [see (B8)] below momenta of $\mathcal{O}(1\ \mathrm{GeV})$, where chiral symmetry breaking is triggered. To take these effects into account we study the STI-consistent version of the most important tensor structures,

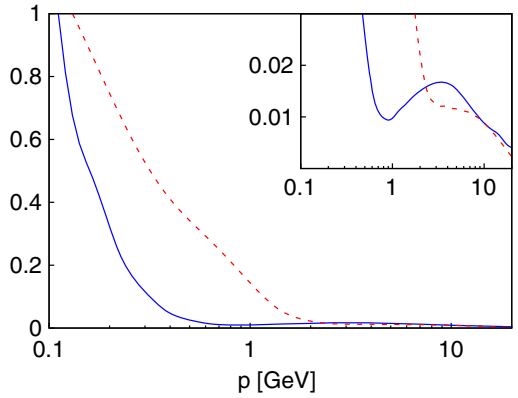

FIG. 6 (color online). Normalized difference $(z^{(7)}_{\bar{q}Aq} - 2z^{(5)}_{\bar{q}Aq})/z^{(7)}_{\bar{q}Aq}$ (blue solid) and $(z_{\bar{c}Ac} - z^{(1)}_{\bar{q}Aq})/z_{\bar{c}Ac}$ (red dashed). Small values indicate that the mSTI is applicable for constraining transversal tensor structures.

$$z^{(5)}_{\bar{q}Aq}(\not{p} + \not{q})(p-q)^\mu, \qquad z^{(7)}_{\bar{q}Aq}\frac{1}{2}[\not{p}, \not{q}]\gamma^\mu \tag{A8}$$

[see Fig. 4(a)]. It can be shown that terms proportional to $z^{(5)}_{\bar{q}Aq}$ and $z^{(7)}_{\bar{q}Aq}$ are derived from

$$z^{(\mathrm{av})}_{\bar{q}Aq}\bar{q}\gamma_5\gamma_\mu\epsilon_{\mu\nu\rho\sigma}D_\nu D_\rho D_\sigma q, \tag{A9}$$

with

$$z^{(7)}_{\bar{q}Aq} = z^{(\mathrm{av})}_{\bar{q}Aq}, \qquad z^{(5)}_{\bar{q}Aq} = \frac{1}{2}z^{(\mathrm{av})}_{\bar{q}Aq}, \tag{A10}$$

valid for constant $z^{(\mathrm{av})}_{\bar{q}Aq}$. In (A9) we have used that the mSTI-consistent extension of the $z^{(5)}_{\bar{q}Aq}, z^{(7)}_{\bar{q}Aq}$-momentum structure in (A8) is

$$\frac{1}{4}\bar{q}D_\mu\{[\gamma_\mu, \gamma_\nu], \not{D}\}D_\nu q. \tag{A11}$$

The tensor structure (A11) only projects on the $z^{(5)}_{\bar{q}Aq}$ and $z^{(7)}_{\bar{q}Aq}$ terms. After some algebra, (A11) can be rewritten as (A9) by using

$$\frac{1}{4}z^{(\mathrm{av})}_{\bar{q}Aq}\{[\gamma_\mu, \gamma_\nu], \gamma_\rho\} = \epsilon_{\mu\nu\rho\alpha}\gamma_5\gamma_\alpha. \tag{A12}$$

With (A7) we get

$$z^{(\mathrm{av})}_{\bar{q}Aq}\frac{i}{4}\sqrt{4\pi\alpha_s}\bar{q}\gamma_5\gamma_\mu\epsilon_{\mu\nu\rho\sigma}\{F_{\nu\rho}, D_\sigma\}q. \tag{A13}$$

Hence, as long as

$$z^{(7)}_{\bar{q}Aq} - 2z^{(5)}_{\bar{q}Aq} = 0, \tag{A14}$$

the quark-gluon vertex tensor structures (A8) follow from the single term (A13), see Fig. 6. This term is derived from the mSTI which is valid down to the semi-perturbative regime. We conclude that within a self-consistent

approximation one also has to take into account the related quark-gluon scattering vertices ($\bar{q}A^2q$ and $\bar{q}A^3q$) derived from (A13). A more detailed study will be published separately. Finally, it is noteworthy that the tensor structure (A13) also plays a crucial rôle in the so-called transverse Ward-Takahashi identity for the quark-gluon vertex, see [63] and e.g. [48,64,65] for applications.

APPENDIX B: TRUNCATION

In this section we discuss in detail the different constituents of the truncation scheme introduced in Sec. II B.

1. Yang-Mills sector

a. Propagators

The only external input which is required in our calculation are the pure gauge propagators. In Landau gauge, the inverse gluon propagator can be parametrized as

$$\Gamma^{\mu\nu}_{A^2}(p) = Z_A(p)p^2\Pi^{\mu\nu}_T(p), \tag{B1}$$

where $\Pi^{\mu\nu}_T(p)$ denotes the transverse projector

$$\Pi^{\mu\nu}_T(p) = \left(\delta^{\mu\nu} - \frac{p^\mu p^\nu}{p^2}\right). \tag{B2}$$

In addition to the gluon propagator we also encounter the ghost propagator,

$$\Gamma_{\bar{c}c}(p) = Z_c(p)p^2, \tag{B3}$$

in the equations for the pure gauge vertices.

We stress that the matter sector computation does not rely on a particular propagator input, but can use any available propagators. This includes RG-scale and momentum-dependent propagators as provided by FRG calculations [15,19] or just momentum-dependent input such as lattice Yang Mills propagators in minimal Landau gauge from [20,22] where the former will be used here, see Fig. 1(a). Taking an external input for the propagators automatically sets the scale of the theory and, apart from the bare quark mass, no parameters remain in the perturbative regime, where we set our initial condition.

b. Vertices

We approximate the ghost-gluon vertex, the three-gluon vertex and the four-gluon vertex with their classical tensor structures and a momentum-dependent dressing, z_X for $X \in \{\bar{c}Ac, A^3, A^4\}$,

$$\begin{aligned}
\Gamma_{\bar{c}Ac}(p_1,p_2)^{abc}_{\mu} &= z_{\bar{c}Ac}(\bar{p})Z_c(\bar{p})Z_A^{1/2}(\bar{p})[\mathrm{i}gf^{abc}q_\mu],\\
\Gamma_{A^3}(p_1,p_2)^{abc}_{\mu\nu\rho} &= z_{A^3}(\bar{p})Z_A^{3/2}(\bar{p})[\mathrm{i}f^{abc}\\
&\quad\times\{(p_2-p_1)_\rho\delta_{\mu\nu}+\mathrm{perm}\}],\\
\Gamma_{A^4}(p_1,p_2,p_3)^{abcd}_{\mu\nu\rho\sigma} &= z_{A^4}(\bar{p})Z_A^2(\bar{p})[f^{iab}f^{icd}\delta_{\mu\rho}\delta_{\nu\sigma}+\mathrm{perm}].
\end{aligned} \tag{B4}$$

Here the p_i, denote the momenta and we approximate the dressing functions z_X as functions of one average momentum $\bar{p} \equiv \sqrt{\sum_i p_i^2/\sum_i}$. To project onto the dressing functions we multiply each gluon leg with the corresponding transversal projector. Therefore, the projection on the ghost-gluon vertex dressing is uniquely defined whereas we contract the three-gluon vertex equation additionally with $\delta_{\mu\nu}p_{2,\rho} - \delta_{\nu\rho}p_{2,\mu}$. The four-gluon vertex is approximated from the three-gluon vertex via

$$z_{A^4}(\bar{p}) = z^2_{A^3}(\bar{p}), \tag{B5}$$

which leads to an approximate agreement of the three-gluon running coupling with the ghost-gluon and quark-gluon running coupling down to $\mathcal{O}(1\ \mathrm{GeV})$ and is still expected to improve with an improved momentum resolution of the glue sector, see the discussion in Sec. III C.

2. Matter sector

a. Quark propagator

We parametrize the inverse dressed quark propagator with two dressing functions as

$$\Gamma_{\bar{q}q}(p) = Z_q(p)(\mathrm{i}\not{p} + M_q(p)), \tag{B6}$$

where

$$\{\gamma_\mu,\gamma_\nu\} = 2\delta_{\mu\nu}\mathbb{1}, \qquad \gamma_\mu^\dagger = \gamma_\mu, \qquad \gamma_5 = \gamma_1\gamma_2\gamma_3\gamma_4. \tag{B7}$$

Setting the current quark mass, $M_q(20\ \mathrm{GeV}) = 1.3\ \mathrm{MeV}$, is related to the value of the pion mass; see Appendix B 2 d. Apart from the purely mesonic sector of our truncation, the full momentum dependence of the quark propagator is fed back into the equations for all other vertices. In the quark-meson sector, as described in Sec. B 2 d, such an approximation leads to an overestimation of the suppression of loops containing quarks via the quark mass function. The resulting effect will most likely be an underestimation of the order parameter $\langle\sigma\rangle$ since the quarks drive the order parameter to larger values in the quark-meson model.

b. Quark-gluon interactions

In Landau gauge, a basis for the quark-gluon vertex is given by the eight tensor structures,

$$
\begin{aligned}
[\mathcal{T}^{(1)}_{\bar{q}Aq}]^\mu(p,q) &= \gamma^\mu,\\
[\mathcal{T}^{(2)}_{\bar{q}Aq}]^\mu(p,q) &= -\mathrm{i}(p-q)^\mu,\\
[\mathcal{T}^{(3)}_{\bar{q}Aq}]^\mu(p,q) &= -\mathrm{i}(\not{p}-\not{q})\gamma^\mu,\\
[\mathcal{T}^{(4)}_{\bar{q}Aq}]^\mu(p,q) &= \mathrm{i}(\not{p}+\not{q})\gamma^\mu,\\
[\mathcal{T}^{(5)}_{\bar{q}Aq}]^\mu(p,q) &= (\not{p}+\not{q})(p-q)^\mu,\\
[\mathcal{T}^{(6)}_{\bar{q}Aq}]^\mu(p,q) &= -(\not{p}-\not{q})(p-q)^\mu,\\
[\mathcal{T}^{(7)}_{\bar{q}Aq}]^\mu(p,q) &= \frac{1}{2}[\not{p},\not{q}]\gamma^\mu,\\
[\mathcal{T}^{(8)}_{\bar{q}Aq}]^\mu(p,q) &= -\frac{\mathrm{i}}{2}[\not{p},\not{q}](p-p)^\mu,
\end{aligned}
\tag{B8}
$$

where p (q) denotes the momentum of the (anti)quark. It is important to note that the tensor structures $\mathcal{T}^{(2)}_{\bar{q}Aq}$, $\mathcal{T}^{(3)}_{\bar{q}Aq}$, $\mathcal{T}^{(4)}_{\bar{q}Aq}$ and $\mathcal{T}^{(8)}_{\bar{q}Aq}$ break chiral symmetry and are only created in the spontaneously broken phase. Our final ansatz for the quark-gluon vertex is then

$$
\begin{aligned}
\Gamma_{\bar{q}Aq}(p,q) = &-\mathrm{i}Z_q(\bar{p})Z_A^{1/2}(\bar{p})\\
&\times\sum_i \frac{z^{(i)}_{\bar{q}Aq}(p,q)}{\bar{p}^{n_i}}[\mathcal{T}^{(i)}_{\bar{q}Aq}]^\mu(p,q),
\end{aligned}
\tag{B9}
$$

where $\bar{p}^{n_i}$ is the average momentum and n_i is chosen such that $z^{(i)}_{\bar{q}Aq}(p,q)$ is dimensionless.

As remarked in Sec. III A a sensible truncation scheme should also include a set of higher-order operators to complete it consistent with the STI. We find that the most important contributions to nonclassical tensor structures in the quark-gluon vertex stem from terms of the form

$$
\bar{q}T_{\mu\nu}D_\mu D_\nu q, \qquad \bar{q}T_{\mu\nu\rho}D_\mu D_\rho D_\nu q, \tag{B10}
$$

where the first (second) contribution breaks (respects) chiral symmetry. In momentum space these yield contributions to the action of the form

$$
\begin{aligned}
&\mathcal{O}(\bar{q}Aq):\ \bar{q}(p)\{T_{\mu\nu}(\mathrm{i}q_\nu)+T_{\nu\mu}(-\mathrm{i}p_\nu)+T_{\mu\nu\rho}(-q_\nu q_\rho)+T_{\nu\mu\rho}(-p_\nu p_\rho)+T_{\rho\nu\mu}(p_\rho q_\nu)\}\times[-\mathrm{i}gA_\mu(-p-q)]q(q),\\
&\mathcal{O}(\bar{q}A^2q):\ \bar{q}(p)\{T_{\mu\nu}+T_{\rho\mu\nu}(-\mathrm{i}p_\rho)+T_{\nu\mu\rho}(\mathrm{i}(r+q)_\rho)+T_{\nu\rho\mu}(\mathrm{i}q_\rho)\}[-\mathrm{i}gA_\nu(-p-q-r)][-\mathrm{i}gA_\mu(r)]q(q),\\
&\mathcal{O}(\bar{q}A^3q):\ \bar{q}(p)T_{\mu\nu\rho}[-\mathrm{i}gA_\mu(-p-q-r+s)]\times[-\mathrm{i}gA_\rho(s)][-\mathrm{i}gA_\nu(r)]q(q),
\end{aligned}
\tag{B11}
$$

where g is to be understood as $g=\sqrt{4\pi\alpha(\bar{p})Z_A(\bar{p})}$ everywhere. In particular, we find that the dominant contributions to order D^2 and D^3 correspond to the tensor structures,

$$
\begin{aligned}
T_{\mu\nu} &= \delta_{\mu\nu}+[\gamma_\mu,\gamma_\nu],\\
T_{\mu\nu\rho} &= \{[\gamma_\mu,\gamma_\nu],\gamma_\rho\}.
\end{aligned}
\tag{B12}
$$

In terms of quark-gluon tensor structures from (B8), these are proportional to the linear combinations

$$
\frac{1}{2}\mathcal{T}^{(2)}_{\bar{q}Aq}+\mathcal{T}^{(4)}_{\bar{q}Aq}, \qquad \frac{1}{2}\mathcal{T}^{(5)}_{\bar{q}Aq}+\mathcal{T}^{(7)}_{\bar{q}Aq} \tag{B13}
$$

[see Fig. 4(a)].

Therefore, we set for consistency reasons $z^{(5)}_{\bar{q}Aq}=\frac{1}{2}z^{(7)}_{\bar{q}Aq}$ and $z^{(2)}_{\bar{q}Aq}=z^{(4)}_{\bar{q}Aq}$ in all equations. The dressing of the corresponding higher-order operators is then simply identified with that of the corresponding quark-gluon vertex dressings $z^{(7)}_{\bar{q}Aq}$ and $z^{(4)}_{\bar{q}Aq}$, respectively, where we additionally use the RG-invariant ansatz as in all other vertices, e.g.

$$
\begin{aligned}
&\bar{q}(p)Z_q(\bar{p})z^{(4)}_{\bar{q}Aq}(\bar{p})T_{\mu\nu}[-\mathrm{i}\sqrt{4\pi\alpha(\bar{p})Z_A(\bar{p})}A_\mu(r)]\\
&\quad\times[-\mathrm{i}\sqrt{4\pi\alpha(\bar{p})Z_A(\bar{p})}A_\nu(-p-q-r)]q(q),
\end{aligned}
\tag{B14}
$$

with $\bar{p}=\sqrt{(p^2+q^2+r^2+(p+q+r)^2)/4}$.

c. Four-Fermi interactions

Here we discuss a basis for the four-Fermi interactions where $(S\pm P)/(V\pm A)$ denotes the scalar-pseudoscalar/vector-axialvector Dirac structure, the subscript denotes the flavor structure and the superscript the color structure. Omitted subscripts and superscripts are to be understood as singlet contributions.

A basis for the $U(2)_L\times U(2)_R$ symmetric four-Fermi interactions is given by [68] (see also [11] for a review),

$$
\begin{aligned}
\mathcal{L}^{(S-P)_+}_{(\bar{q}q)^2} &= (\bar{q}T^0q)^2-(\bar{q}\gamma^5T^fq)^2-(\bar{q}\gamma^5T^0q)^2+(\bar{q}T^fq)^2\\
\mathcal{L}^{(V-A)}_{(\bar{q}q)^2} &= (\bar{q}\gamma^\mu T^0q)^2+(\bar{q}\gamma^\mu\gamma^5T^0q)^2\\
\mathcal{L}^{(V+A)}_{(\bar{q}q)^2} &= (\bar{q}\gamma^\mu T^0q)^2-(\bar{q}\gamma^\mu\gamma^5T^0q)^2\\
\mathcal{L}^{(V-A)^{\mathrm{adj}}}_{(\bar{q}q)^2} &= (\bar{q}\gamma^\mu T^0T^aq)^2+(\bar{q}\gamma^\mu\gamma^5T^0T^aq)^2.
\end{aligned}
\tag{B15}
$$

We denote the generators of flavor $U(1)$ and $SU(2)$ by T^0 and T^f whereas T^a are the generators of color $SU(3)_c$. Note, that the obvious choice $(S-P)^{\text{adj}}_{+}$ instead of $(V-A)^{\text{adj}}$ is not linearly independent of $(S-P)_+$ and $(V+A)$ and, therefore, $(V-A)^{\text{adj}}$ has to be considered.

There are two four-Fermi interactions which break the axial $U(1)_A$ but are symmetric under $U(1)_V \times SU(2)_L \times SU(2)_R$

$$\begin{aligned}\mathcal{L}^{(S+P)_-}_{(\bar{q}q)^2} &= (\bar{q}T^0 q)^2 - (\bar{q}\gamma^5 T^f q)^2 + (\bar{q}\gamma^5 T^0 q)^2 - (\bar{q}T^f q)^2 \\ \mathcal{L}^{(S+P)^{\text{adj}}_-}_{(\bar{q}q)^2} &= (\bar{q}T^0 T^a q)^2 - (\bar{q}\gamma^5 T^f T^a q)^2 \\ &\quad + (\bar{q}\gamma^5 T^0 T^a q)^2 - (\bar{q}T^f T^a q)^2, \end{aligned} \tag{B16}$$

where the first corresponds to the 't Hooft determinant [69]. For applications it is convenient to introduce the linear combinations,

$$\begin{aligned}\mathcal{L}^{(\pi)}_{(\bar{q}q)^2} &= \mathcal{L}^{(S-P)_+}_{(\bar{q}q)^2} + \mathcal{L}^{(S+P)_-}_{(\bar{q}q)^2} = 2(\bar{q}T^0 q)^2 - 2(\bar{q}\gamma^5 T^f q)^2 \\ \mathcal{L}^{(\eta')}_{(\bar{q}q)^2} &= \mathcal{L}^{(S-P)_+}_{(\bar{q}q)^2} - \mathcal{L}^{(S+P)_-}_{(\bar{q}q)^2} = 2(\bar{q}T^f q)^2 - 2(\bar{q}\gamma^5 T^0 q)^2, \end{aligned} \tag{B17}$$

with quantum numbers corresponding to $(\sigma-\pi)-$ and $(\eta-a)-$ meson exchange channels.

Since the $SU(2)_L \times SU(2)_R$ symmetry is only approximate and explicitly broken to $SU(2)_{L+R}$, we additionally take into account the tensor structures,

$$\begin{aligned}\mathcal{L}^{(S+P)_+}_{(\bar{q}q)^2} &= (\bar{q}T^0 q)^2 + (\bar{q}\gamma^5 T^f q)^2 + (\bar{q}\gamma^5 T^0 q)^2 + (\bar{q}T^f q)^2 \\ \mathcal{L}^{(S+P)^{\text{adj}}_+}_{(\bar{q}q)^2} &= (\bar{q}T^0 T^a q)^2 + (\bar{q}\gamma^5 T^f T^a q)^2 \\ &\quad + (\bar{q}\gamma^5 T^0 T^a q)^2 + (\bar{q}T^f T^a q)^2, \end{aligned} \tag{B18}$$

which break $SU(2)_A$. Finally, there are two basis elements which break $SU(2)_A$ as well as $U(1)_A$:

$$\begin{aligned}\mathcal{L}^{(S-P)_-}_{(\bar{q}q)^2} &= (\bar{q}T^0 q)^2 + (\bar{q}\gamma^5 T^f q)^2 - (\bar{q}\gamma^5 T^0 q)^2 - (\bar{q}T^f q)^2 \\ \mathcal{L}^{(S-P)^{\text{adj}}_-}_{(\bar{q}q)^2} &= (\bar{q}T^0 T^a q)^2 + (\bar{q}\gamma^5 T^f T^a q)^2 \\ &\quad - (\bar{q}\gamma^5 T^0 T^a q)^2 - (\bar{q}T^f T^a q)^2. \end{aligned} \tag{B19}$$

Consequently, a basis that respects $U(1)_V \times SU(2)_V$ consists of ten elements and the ansatz for the full four-Fermi vertex is given by

$$\Gamma_{(\bar{q}q)^2,k}(p_1,p_2,p_3) = Z^2_{q,k}(0)\sum_i \frac{\lambda_{i,k}(s)}{k^2}\mathcal{L}^i_{(\bar{q}q)^2}, \tag{B20}$$

where the sum runs over these ten tensor structures. We investigated the momentum dependencies in the four-Fermi interactions for three momentum configurations corresponding to pure s-, t- and u-channel momentum configurations on the basis of the given solution at zero external momentum. For example, for the s channel we consider $p_1 = p_2 = -p_3 = -p_4 = p$ corresponding to $s = 4p^2$.

d. Quark-meson system: LPA′ approximation

We parametrize the inverse meson propagators as

$$\Gamma_{\sigma^2/\vec{\pi}^2,k}(p) = Z_{\pi,k}(p^2 + m^2_{\sigma/\pi,k}). \tag{B21}$$

In the chirally symmetric phase, the approximation $Z_\sigma \approx Z_\pi$ is exact, whereas the deviations in the broken phase are suppressed by the comparably large mass of the sigma-meson m_σ. The mass terms can be absorbed into the definition of the effective mesonic potential and will be discussed there. Additionally we neglect the momentum dependence of Z_π which has been shown to be a quantitatively reliable approximation [6]. As a consequence, only the anomalous dimension,

$$\eta_\pi = -\frac{\partial_t Z_\pi}{Z_\pi}, \tag{B22}$$

appears in any of the flow equations.

We perform a Taylor expansion of the effective mesonic potential in ρ [70],

$$V(\bar{\rho} \equiv Z_\pi \rho) = \sum_{j=0}^{6} \frac{v_j}{j!}(\bar{\rho} - \bar{\rho}_0)^j, \tag{B23}$$

with $\bar{\rho}_0 \equiv Z_\pi \rho_0$ and ρ_0 scale independent such that $\bar{\rho}_0$ becomes the minimum of the effective potential at $k \to 0$. At this order of the Taylor expansion we see convergence and a comparison to a calculation on a discrete grid in ρ yields perfect agreement. The meson masses are obtained from this potential as

$$\begin{aligned} m^2_\pi &= V'(\bar{\rho}_0), \\ m^2_\sigma &= V'(\bar{\rho}_0) + 2\bar{\rho}_0 V''(\bar{\rho}_0). \end{aligned} \tag{B24}$$

Therefore, the value of the pion mass depends directly on the expansion point $\bar{\rho}_0$ which, in turn, is directly proportional to the current quark mass $M_q(\Lambda)$. In our case we choose $M_q(20\ \text{GeV}) = 1.3$ MeV such that m_π takes the physical value of 135 MeV.

We consider only one Yukawa interaction of the $\sigma-\pi$ tensor structure $\mathcal{L}^{(\pi)}_{(\bar{q}q)^2}$. Hence, integrating out the mesonic fields leads to contributions to the four-Fermi interaction $\mathcal{L}^{(\pi)}_{(\bar{q}q)^2}$. In other words, the total coupling of $\mathcal{L}^{(\pi)}_{(\bar{q}q)^2}$ is a sum of the explicit four-Fermi interaction and the part stored in the quark-meson sector of the theory. The distribution of

these fluctuations is done with dynamical hadronization explained in Appendix D.

The chirally symmetric Yukawa interaction reads

$$\int_{p_1,p_2} z_{\bar{q}\phi q}(p_1,p_2)\bar{Z}_\pi^{\frac{1}{2}}(p_1+p_2)\bar{Z}_q^{\frac{1}{2}}(p_1)\bar{Z}_q^{\frac{1}{2}}(p_2) \times \phi(p_1+p_2)\bar{q}(p_1)\tau q(p_2), \tag{B25}$$

where $\tau=(T^0,\gamma_5\vec{T})$. Reducing this to the s channel with $p_1=p_2=p$ leads to

$$\int_p z_{\bar{q}\phi q}(p,p)\bar{Z}_\pi^{\frac{1}{2}}(2p)\bar{Z}_q^{\frac{1}{2}}(p)\bar{Z}_q^{\frac{1}{2}}(p)\times\phi(2p)\bar{q}(p)\tau q(p). \tag{B26}$$

In our calculations we use the renormalized Yukawa coupling h_π, with $\bar{Z}_\pi(2p)\equiv Z_{\pi,k}(0)$, $\bar{Z}_q(p)\equiv\bar{Z}_{q,k}(0)$ and

$$h_\pi(2p)=2z_{\bar{q}\phi q}(p,p), \tag{B27}$$

where $2p$ is the momentum of the mesonic field $\phi(2p)$. Furthermore, we ignore momentum dependencies as well as field dependencies in h_π.

This parametrization of the quark-meson model is termed "LPA′ approximation" and has been shown to be capable of approximating the full momentum dependence very well [6]. Furthermore, it has been found that the effect of higher meson quark interactions that stem from a possible field dependence in the Yukawa interaction would yield a decrease of the order of 10% in the chiral condensate [70].

APPENDIX C: STABILITY OF THE TRUNCATION

Here we give a detailed analysis of the systematic errors and hence of the stability of the current truncation. To this end we briefly summarize the vertex structures taken into account: in the pure gauge sector, the classical tensor structures of all primitively divergent correlation functions have been considered. The quark propagator and the quark-gluon vertex—as the essential interface coupling between glue and matter sector—have been included with full momentum dependencies and all tensor structures. Additionally, higher quark-gluon interactions as obtained from a gauge invariant extension of nonclassical tensors structures in the quark-gluon vertex have been taken into account. A Fierz-complete basis has been used for the four-Fermi couplings in an s-channel approximation. Moreover, meson propagators and quark-meson Yukawa interactions, as well as higher-order mesonic correlation functions in the scalar-pseudoscalar s channel, are included.

Gluonic interactions: As the momentum dependence of the Yang-Mills vertices has been found to be rather small at the relevant momentum scales [30–35,66,67,71], we approximated the momentum dependence of these vertices only with one variable at the symmetric point, which is expected to be a good approximation.

For the three-gluon vertex, DSE studies show that the effect of additional tensors structures is small [32]. Furthermore, there exists only one nonclassical gauge invariant operator contributing to the three-gluon vertex that can be constructed from the field strength tensor, namely, $\mathrm{tr}[F_{\mu\nu}F_{\nu\rho}F_{\rho\mu}]$. We explicitly calculated its dressing and found it to be negligibly small. In the ghost-gluon vertex, on the other hand, only one (transversal) tensor structure contributes in Landau gauge. Our largest systematic error concerns, therefore, the four-gluon vertex which has been determined via STIs from the three-gluon vertex keeping only the classical tensor structure. While this certainly works well in the semi-perturbative regime, below $\mathcal{O}(1\ \mathrm{GeV})$ deviations are to be expected as well as contributions from other tensor structures (see [35]). Indeed, the three-gluon vertex running coupling deviates already earlier from the other running couplings, indicating some missing vertex strength [see Fig. 4(b)].

Quark-gluon interactions: In the matter sector the quark-gluon vertex was fully taken into account. However, based on an analysis of the relative strength of the different tensor structures we only fed back the $\mathcal{T}^{(4)}_{\bar{q}Aq}$ and $\mathcal{T}^{(7)}_{\bar{q}Aq}$ as the dominant chiral symmetry breaking and chiral tensor structures. We have checked the quantitative convergence of this approximation at the example of the flow equations of the quark propagator and the quark-gluon vertex itself.

Higher quark-gluon interactions follow from the quark-gluon vertex using the modified Slavnov-Taylor identities (mSTIs) discussed in Appendix A. The applicability of the mSTIs, which constrain only the longitudinal part of any correlation function, relies on identifying them with their transversal counterparts. At nonperturbative momenta $\mathcal{O}(1\ \mathrm{GeV})$, the connection between transversal and longitudinal parts is lost, with the running couplings as obtained from different vertices as a prominent example; see comparison of $z^{(1)}_{\bar{q}Aq}\alpha\sqrt{\alpha_{\bar{q}Aq}}$ with $z_{\bar{c}Ac}\alpha\sqrt{\alpha_{\bar{c}Ac}}$ in Fig. 6. In their regime of applicability, the mSTIs provide, therefore, relations between different tensor structures—most prominently this leads to $z^{(7)}_{\bar{q}Aq}-2z^{(5)}_{\bar{q}Aq}\approx 0$—see Appendix A 2. In Fig. 6 we show the normalized difference $(z^{(7)}_{\bar{q}Aq}-2z^{(5)}_{\bar{q}Aq})/z^{(7)}_{\bar{q}Aq}$ as obtained from the vertex equation with only the classical tensor structure inserted on the right-hand side. In this case the mSTI is fulfilled even better than for the strong running coupling down to very low momenta $\mathcal{O}(0.5\ \mathrm{GeV})$. We take this as a justification for approximating the dressing and momentum dependence of the higher quark-gluon interactions by the solution of the semi-perturbative mSTI that relates them to the tensor structure $\frac{1}{2}\mathcal{T}^{(5)}_{\bar{q}Aq}+\mathcal{T}^{(7)}_{\bar{q}Aq}$.

Quark interactions: We have taken into account a complete Fierz basis for the four-Fermi interaction and

used s-channel approximations for all tensor structures. All higher purely fermionic vertices in the s channel of the scalar-pseudoscalar interaction are included. Their contribution beyond meson exchange (eight-fermion interaction) is small (see [3]). This observation is additionally supported by the fast convergence of expansions in powers of the mesonic field that is found in the quark-meson model and in dynamical QCD, at vanishing temperature [6,70]. Concerning the quark-meson interactions, we neglected higher contributions due to field-derivatives of the Yukawa interaction which have been found to be of the order of 10% [3,70]. A more detailed study will be presented elsewhere.

In the equation for the quark propagator, momentum dependencies of the four-Fermi interactions play a quantitative rôle via the tadpole diagrams. We have implemented this momentum dependence via one momentum variable using a symmetric projection. Furthermore, momentum dependencies in the meson sector have been ignored which is justified by the success of the LPA′ approximation [6]. Additionally, we have ignored the backcoupling of the momentum dependence of the quark propagator in the equation for the effective potential. We expect some effects due to this approximation, which would mitigate the effect of ignoring higher quark-meson interactions.

APPENDIX D: DYNAMICAL HADRONIZATION

As already pointed out in the main text, the concept of dynamical hadronization [8,24,25] is of crucial importance for the present application. In the form used here, it allows us to exactly rewrite momentum channels of the four-Fermi interactions in terms of Yukawa couplings to an effective bosonic exchange field. This corresponds to a Hubbard-Stratonovich transformation in every RG-step, and is also called rebosonization in the present case of composite bosonic fields [24]. Naturally, the bosonic field carries the quantum numbers of the related four-Fermi channel, and may be interpreted as the corresponding meson or diquark field.

For simplicity, we restrict ourselves in the following discussion to the dynamical hadronization of the sigma-pion channel. Following [8] and in particular [3], we start from the path integral representation for $\Gamma_k[\Phi]$ in terms of the fundamental superfield $\hat{\varphi} = (\hat{A}_\mu, \hat{C}, \hat{\bar{C}}, \hat{q}, \hat{\bar{q}})$,

$$e^{-\Gamma_k[\Phi]} = \int \mathcal{D}\hat{\varphi} e^{-S[\hat{\varphi}]-\Delta S_k[\hat{\phi}_k]+\frac{\delta(\Gamma_k+\Delta S_k)}{\delta\hat{\phi}}(\hat{\Phi}_k-\Phi)+\Delta S_k[\Phi]}, \quad \text{(D1)}$$

with $\Delta S_k[\Phi] = \frac{1}{2}\Phi R_k \Phi$, where we introduced a dynamical superfield $\hat{\Phi}_k = (\hat{\varphi}, \hat{\sigma}_k, \hat{\vec{\pi}}_k)$ with expectation value $\Phi = \langle\hat{\Phi}_k\rangle \equiv (\varphi, \sigma, \vec{\pi})$. It is constructed from the fundamental superfield φ and scale-dependent composite operators $\hat{\phi}_k = (\hat{\sigma}_k, \hat{\vec{\pi}}_k)$, whose flow we define to be of the form

$$\partial_t\hat{\phi}_k(r) = \partial_t A_k(r)(\bar{q}\tau q)(r) + \partial_t B_k(r)\hat{\phi}_k(r) \quad \text{(D2)}$$

with $(\bar{q}\tau q)(r) = \int_l \bar{q}(l)\tau q(r-l)$. The flow (D2) is defined in momentum space which will allow us to identify it with a specific momentum channel in the four-Fermi flow. Note also that the term multiplying $\partial_t A_k$ involves only expectation values q and $\bar{q}$. The two coefficient functions $\partial_t A_k$ and $\partial_t B_k$ appearing in (D2) are so far undetermined and at our disposal in the dynamical hadronization. They specify the RG-adaptive change of our field basis. The scale dependence of $\hat{\phi}_k$ leads to additional contributions on the right-hand side of the flow equation compared to (1), which now takes the form

$$\partial_t|_\phi\Gamma_k[\Phi] = \frac{1}{2}\mathrm{Tr}\frac{1}{\Gamma_k^{(2)}+R_k}(\partial_t R_k + 2R_k\partial_t B_k) - \int_l \frac{\delta\Gamma_k}{\delta\phi}[\partial_t A_k(r)(\bar{q}\tau q)(r) + \partial_t B_k(r)\phi(r)]. \quad \text{(D3)}$$

The second line on the right-hand side accounts for the scale dependence of the composite fields. Together with the left-hand side, they constitute a total derivative with respect to the logarithmic scale t. In the present work, we use $\partial_t A_k(r)$ to completely eliminate the corresponding channel of the scalar-pseudoscalar four-Fermi interaction with $\lambda_\pi \equiv \lambda_{(S-P)_+} + \lambda_{(S+P)_-}$ and $\lambda_\pi(s) = \lambda_\pi(p,p,-p)$ [see (B20)], that is, with $t = u = 0$,

$$\partial_t\lambda_\pi(s) = \mathrm{Flow}_\pi^{(4)}(s) - \partial_t A_k(2p)h_\pi(2p) \stackrel{!}{=} 0, \quad \text{(D4)}$$

where $\mathrm{Flow}_\pi^{(4)}(s)$ stands for the diagrams in the four-Fermi flow. Equation (D4) leads to a vanishing flow of the s channel of the four-Fermi coupling λ_π and requires

$$\partial_t A_k(2p) = \frac{\mathrm{Flow}_\pi^{(4)}(s)}{h(2p)}, \quad \text{with} \quad s = 4p^2, \quad \text{(D5)}$$

which completely fixes $\partial_t A_k(2p)$. Still, the second rebosonization function $\partial_t B_k(2p)$ is at our disposal. It can be used to improve the approximation at hand by distributing the momentum dependence of the rebosonized four-Fermi channel between the Yukawa coupling and the mesonic propagator. For example, when considering the full momentum dependence of the latter but only a running, momentum-independent Yukawa coupling, the $\partial_t B_k$ can be chosen such that this is an exact procedure. The discussion of the general procedure is beyond the scope of the present work and will be presented elsewhere. In the present case we resort to the simplest option by using

$$\partial_t B_k \equiv 0. \quad \text{(D6)}$$

As a consequence of (D3) together with (D5) and (D6) we get additional contributions to the mesonic anomalous

dimension at vanishing momentum and the momentum-dependent quark-meson coupling $h_\pi(2p)$,

$$\partial_t \Delta\eta_\pi = 2\frac{V'(\bar{\rho}_0)}{h_\pi^2(0)}\mathrm{Flow}_\pi^{(4)}(0),$$
$$\partial_t \Delta h_\pi(2p) = \frac{\Gamma_\pi^{(2)}(2p)}{h_\pi(2p)}\mathrm{Flow}_\pi^{(4)}(s). \quad \text{(D7)}$$

The quark mass function is directly related to the quark-meson coupling, $M_q(p) = \langle\sigma\rangle h_\pi(2p)/2$. Moreover, in the current approximation, we use a constant $h_\pi = h_\pi(0)$ on the right-hand side of the flows. With $\Gamma_\pi^{(2)}(0) = V'(\bar{\rho}_0)$ this leads us to

$$\partial_t \Delta h_\pi(0) = \frac{V'(\bar{\rho}_0)}{h_\pi(0)}\mathrm{Flow}_\pi^{(4)}(0), \quad \text{(D8)}$$

$$\partial_t \Delta M_q(p) = M_q(p)\frac{V'(\bar{\rho}_0)}{h_\pi(0)^2}\frac{\bar{\lambda}_\pi(0)}{\bar{\lambda}_\pi(s)}\partial_t\bar{\lambda}_\pi(s), \quad \text{(D9)}$$

with

$$\bar{\lambda}_\pi(s) = \int_{\Lambda_{\mathrm{UV}}}^{k}\frac{dk'}{k'}\mathrm{Flow}_\pi^{(4)}(s). \quad \text{(D10)}$$

In (D9) we have used that

$$\frac{\Gamma_\pi^{(2)}(2p)}{(h_\pi(2p))^2} \approx \frac{V'(\bar{\rho}_0)}{h_\pi(0)^2}\frac{\bar{\lambda}_\pi(0)}{\bar{\lambda}_\pi(s)} \quad \text{(D11)}$$

up to higher-order terms in the mesonic potential. In the present approximation we have a better access to the momentum dependence of $\bar{\lambda}_\pi$ than on that of $\Gamma_\pi^{(2)}$ and h_π. Consequently, using (D9) minimizes the error in our computation of $M_q(p)$. For future work, it would, however, be preferable to calculate the momentum dependence of the right-hand side directly from momentum dependencies in the mesonic sector.

[1] J. Braun, Eur. Phys. J. C **64**, 459 (2009).
[2] J. Braun, L. M. Haas, F. Marhauser, and J. M. Pawlowski, Phys. Rev. Lett. **106**, 022002 (2011).
[3] J. Braun, L. Fister, J. M. Pawlowski, and F. Rennecke, arXiv:1412.1045.
[4] J. Braun, L. Fister, T. Herbst, M. Mitter, J. M. Pawlowski, F. Rennecke, and N. Strodthoff (fQCD Collaboration).
[5] T. K. Herbst, M. Mitter, J. M. Pawlowski, B.-J. Schaefer, and R. Stiele, Phys. Lett. B **731**, 248 (2014).
[6] A. J. Helmboldt, J. M. Pawlowski, and N. Strodthoff, arXiv:1409.8414.
[7] J. Berges, N. Tetradis, and C. Wetterich, Phys. Rep. **363**, 223 (2002).
[8] J. M. Pawlowski, Ann. Phys. (Amsterdam) **322**, 2831 (2007).
[9] H. Gies, Lect. Notes Phys. **852**, 287 (2012).
[10] B.-J. Schaefer and J. Wambach, Phys. Part. Nucl. **39**, 1025 (2008).
[11] J. Braun, J. Phys. G **39**, 033001 (2012).
[12] R. Alkofer and L. von Smekal, Phys. Rep. **353**, 281 (2001).
[13] C. D. Roberts and S. M. Schmidt, Prog. Part. Nucl. Phys. **45**, S1 (2000).
[14] C. S. Fischer, J. Phys. G **32**, R253 (2006).
[15] C. S. Fischer, A. Maas, and J. M. Pawlowski, Ann. Phys. (Amsterdam) **324**, 2408 (2009).
[16] D. Binosi and J. Papavassiliou, Phys. Rep. **479**, 1 (2009).
[17] A. Maas, Phys. Rep. **524**, 203 (2013).
[18] P. Boucaud, J. P. Leroy, A. L. Yaouanc, J. Micheli, O. Pene, and J. Rodríguez-Quintero, Few Body Syst. **53**, 387 (2012).
[19] L. Fister and J. M. Pawlowski (to be published).
[20] P. O. Bowman, U. M. Heller, D. B. Leinweber, M. B. Parappilly, and A. G. Williams, Phys. Rev. D **70**, 034509 (2004).
[21] P. O. Bowman, U. M. Heller, D. B. Leinweber, M. B. Parappilly, A. G. Williams, and J. Zhang, Phys. Rev. D **71**, 054507 (2005).
[22] A. Sternbeck, E. M. Ilgenfritz, M. Muller-Preussker, A. Schiller, and I. L. Bogolubsky, *Proc. Sci.*, LAT (2006) 076.
[23] C. Wetterich, Phys. Lett. B **301**, 90 (1993).
[24] H. Gies and C. Wetterich, Phys. Rev. D **65**, 065001 (2002).
[25] S. Floerchinger and C. Wetterich, Phys. Lett. B **680**, 371 (2009).
[26] Extension of DoFun [27] that utilizes Form [28] and FormLink [29] for the derivation and numerical solution of the flow equations.
[27] M. Q. Huber and J. Braun, Comput. Phys. Commun. **183**, 1290 (2012).
[28] J. Vermaseren, arXiv:math-ph/0010025.
[29] F. Feng and R. Mertig, arXiv:1212.3522.
[30] M. Pelaez, M. Tissier, and N. Wschebor, Phys. Rev. D **88**, 125003 (2013).
[31] A. Blum, M. Q. Huber, M. Mitter, and L. von Smekal, Phys. Rev. D **89**, 061703 (2014).
[32] G. Eichmann, R. Williams, R. Alkofer, and M. Vujinovic, Phys. Rev. D **89**, 105014 (2014).
[33] D. Binosi, D. Ibanez, and J. Papavassiliou, J. High Energy Phys. 09 (2014) 059.
[34] J. Gracey, Phys. Rev. D **90**, 025014 (2014).
[35] A. K. Cyrol, M. Q. Huber, and L. von Smekal, arXiv: 1408.5409.

[36] C. S. Fischer and J. M. Pawlowski, Phys. Rev. D **80**, 025023 (2009).
[37] B.-J. Schaefer and J. Wambach, Nucl. Phys. **A757**, 479 (2005).
[38] C. S. Fischer and R. Alkofer, Phys. Rev. D **67**, 094020 (2003).
[39] D. Jungnickel and C. Wetterich, Phys. Rev. D **53**, 5142 (1996).
[40] B.-J. Schaefer and J. Wambach, Phys. Rev. D **75**, 085015 (2007).
[41] M. Mitter and B.-J. Schaefer, Phys. Rev. D **89**, 054027 (2014).
[42] R. Alkofer, A. Bender, and C. D. Roberts, Int. J. Mod. Phys. A **10**, 3319 (1995).
[43] C. S. Fischer, D. Nickel, and J. Wambach, Phys. Rev. D **76**, 094009 (2007).
[44] C. S. Fischer, D. Nickel, and R. Williams, Eur. Phys. J. C **60**, 47 (2009).
[45] I. Cloet, G. Eichmann, B. El-Bennich, T. Klahn, and C. Roberts, Few Body Syst. **46**, 1 (2009).
[46] M. Hopfer, A. Windisch, and R. Alkofer, *Proc. Sci.*, ConfinementX (2012) 073.
[47] R. Williams, arXiv:1404.2545.
[48] A. Aguilar, D. Binosi, D. Ibanez, and J. Papavassiliou, Phys. Rev. D **90**, 065027 (2014).
[49] R. Alkofer, C. S. Fischer, F. J. Llanes-Estrada, and K. Schwenzer, Ann. Phys. (Amsterdam) **324**, 106 (2009).
[50] J. Pawlowski, Phys. Rev. D **58**, 045011 (1998).
[51] D. Zappala, Phys. Lett. A **290**, 35 (2001).
[52] H. Gies and C. Wetterich, Phys. Rev. D **69**, 025001 (2004).
[53] H. Gies, J. Jaeckel, and C. Wetterich, Phys. Rev. D **69**, 105008 (2004).
[54] H. Gies and J. Jäckel, Eur. Phys. J. C **46**, 433 (2006).
[55] J. Braun and H. Gies, Phys. Lett. B **645**, 53 (2007).
[56] J. Braun and H. Gies, J. High Energy Phys. 06 (2006) 024.
[57] J. M. Pawlowski, AIP Conf. Proc. **1343**, 75 (2011).
[58] L. M. Haas, R. Stiele, J. Braun, J. M. Pawlowski, and J. Schaffner-Bielich, Phys. Rev. D **87**, 076004 (2013).
[59] J. M. Pawlowski, Nucl. Phys. **A931**, 113 (2014).
[60] U. Ellwanger, Phys. Lett. B **335**, 364 (1994).
[61] M. D'Attanasio and T. R. Morris, Phys. Lett. B **378**, 213 (1996).
[62] Y. Igarashi, K. Itoh, and H. So, Prog. Theor. Phys. **106**, 149 (2001).
[63] K.-I. Kondo, Int. J. Mod. Phys. A **12**, 5651 (1997).
[64] S.-X. Qin, L. Chang, Y.-X. Liu, C. D. Roberts, and S. M. Schmidt, Phys. Lett. B **722**, 384 (2013).
[65] S.-X. Qin, C. D. Roberts, and S. M. Schmidt, Phys. Lett. B **733**, 202 (2014).
[66] L. Fister and J. M. Pawlowski, arXiv:1112.5440.
[67] L. Fister, Ph.D. thesis, Heidelberg University, 2012.
[68] J. Jaeckel and C. Wetterich, Phys. Rev. D **68**, 025020 (2003).
[69] G. 't Hooft, Phys. Rev. D **14**, 3432 (1976).
[70] J. M. Pawlowski and F. Rennecke, Phys. Rev. D **90**, 076002 (2014).
[71] M. Q. Huber and L. von Smekal, J. High Energy Phys. 04 (2013) 149.

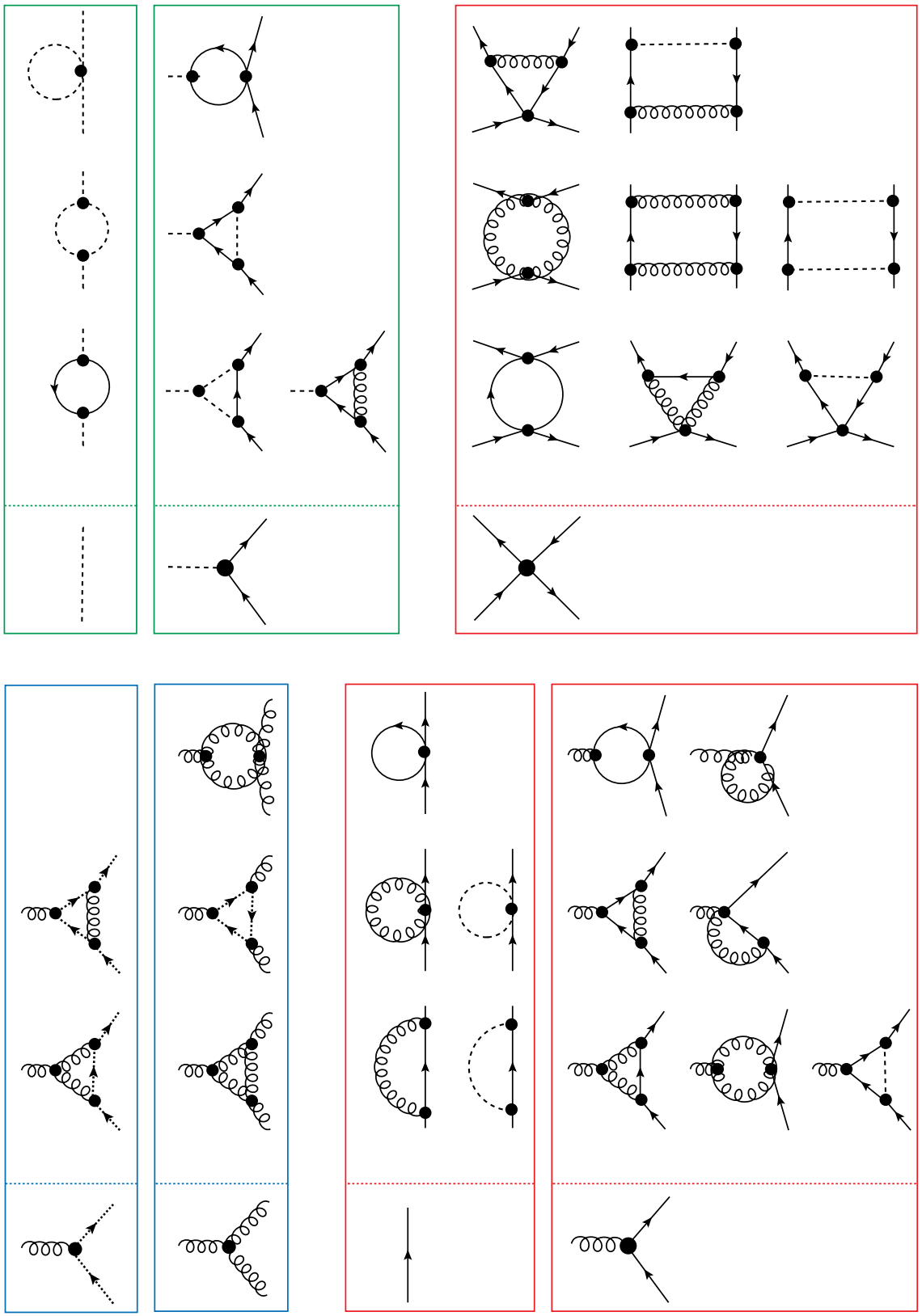

FIG. 7 (color online). Types of diagrams that contribute to flow of propagators and vertices. Quark (solid lines), gluon (wiggly lines), ghost (dotted lines) and meson (dashed lines) propagators as well as the (1PI) vertices are dressed. Each diagram represents a sum of diagrams with (anti)symmetric permutations and regulator function inserted once in each internal propagator line. Symmetry factors and signs are not shown for better readability. Not shown are the flows of ghost and gluon propagators (see [66,67]) as well as those of the effective potential.